HHS Public Access

Author manuscript

J Immunol. Author manuscript; available in PMC 2018 April 01.

Published in final edited form as:

J Immunol. 2017 April 01; 198(7): 2886–2897. doi:10.4049/jimmunol.1601810.

Neutrophil microparticles deliver active myeloperoxidase to injured mucosa to inhibit epithelial wound healing

Thomas W. Slater, **Ariel Finkielsztein**, **Lorraine A. Mascarenhas**, **Lindsey C. Mehl**, **Veronika Butin-Israeli**, and **Ronen Sumagin***

Northwestern University, Feinberg School of Medicine, Department of Pathology, Chicago, IL

Abstract

Neutrophil (PMN) infiltration of the intestinal mucosa often leads to severe epithelial injury, however how this process occurs is unclear. The current work describes a novel mechanism, whereby membrane derived microparticles released by tissue infiltrating PMNs (PMN-MPs) serve as shuttles to protect and deliver active mediators to locally modulate cellular function during inflammation. Specifically, myeloperoxidase (MPO), which is abundantly expressed in PMN azurophilic granules and used for microbial killing, was found to be mobilized to the PMN surface and subsequently released in association with PMN-MPs upon PMN activation and binding to intestinal epithelial cells (IECs). The enzymatic activity of PMN-MP-associated MPO was enhanced compared to soluble protein, leading to potent inhibition of wound closure following PMN-MP binding to IECs. Importantly, localized microinjection of PMN-MPs into wounded colonic mucosa was sufficient to impair epithelial wound healing *in vivo*. PMN-MPs/MPO-dependent inhibition of IEC wound healing was due to impaired IEC migration and proliferation, resulting from impeded actin dynamics, cell spreading, and cell cycle arrest. Thus, our findings provide new insight into mechanisms governing PMN-induced tissue injury, and implicate PMN-MPs and MPO as important regulators of cellular function.

INTRODUCTION

Epithelial cells lining the lumen of the gastrointestinal tract form a barrier that separates its contents from the underlying tissue (1, 2). Epithelial injury and impaired barrier function resulting from non-resolving inflammatory responses are common pathological features of gastrointestinal diseases, including Inflammatory Bowel Diseases (IBD) (2, 3). Efficient epithelial wound healing is critical for the reestablishment of the barrier function and restoration of tissue homeostasis (4). Closure of mucosal wounds involves epithelial cell proliferation and migration (5). Unlike immune cells or fibroblasts, epithelial cells migrate as a cohesive sheet, where forward movement is achieved via coordinated cell polarization

***Corresponding author:** Ronen Sumagin, PhD. Northwestern University, Tarry Research Building, Room: 3-707. 303 E. Chicago Avenue, Chicago, IL, 60611 Ph: 312-503-4468. ronen.sumagin@northwestern.edu.

AUTHOR CONTRIBUTIONS

TS, RS conceived the studies. TS, AF, LM, LM, VBI optimized and conducted the experiments and drafted the manuscript. RS directed the studies and finalized drafting of the manuscript. All of the authors contributed to evaluating and interpreting the data.

DISCLOSURE

The authors declared no conflict of interest.

in the direction of the wound (6), restructuring of the actin cytoskeleton (7), and the extension of cellular membrane protrusions by the leading edge cells (8).

Another important feature of IBD is *en masse* neutrophil (PMN) infiltration of the intestinal epithelium and their accumulation in the intestinal lumen (9, 10). PMNs play a vital role in host defense, however dysregulated PMN recruitment is often associated with exacerbated inflammation and injury. Particularly in IBD, the number of PMNs in the intestinal mucosa has been correlated with severity of the disease (11).

PMN-induced tissue injury is often associated with the release of a variety of PMN-derived soluble mediators. Specifically, metaloproteinases (MMPs), membrane-anchored disintegrin metalloproteinases (ADAMs) and neutrophil elastase (NE) are well known for their ability to modify extracellular, soluble or membrane-bound proteins to promote their rapid delivery or inactivation (12). Myeloperoxidase (MPO) is another enzyme released by tissue infiltrating PMNs that has been linked to tissue damage in both acute and chronic inflammation (13).

MPO is a heme-containing enzyme that is abundantly expressed in PMNs (accounting for up to 5% of total cell protein) and to a lesser degree in monocytes and subtypes of tissue macrophages (14). In the presence of hydrogen peroxide (H_2O_2) and low-molecular-weight intermediates, such as chloride, tyrosine, or nitrite, MPO catalyzes the formation of potent reactive oxygen species (ROS), such as hypochlorous acid (HOCl), tyrosyl radical, and reactive nitrogen intermediates (15). While MPO plays a key role in the killing of ingested bacteria (16), when released into tissues it promotes oxidative tissue damage. As such, MPO and its products have been linked to various diseases including, atherosclerosis, coronary artery disease, Arthritis Alzheimer's and IBD (17–20).

Intriguingly, recent proteome analysis revealed MPO association with PMN-derived microparticles (MPs) also termed microvesicles or ectosomes (21). MPs are vesicles that bud off cell membranes, ranging from 100–1000 nm in diameter. MP release by leukocyte subtypes, platelets, endothelial and epithelial cells in response to cellular activation has recently emerged as a new means for cell-to-cell communication and protein transport (22). Importantly, MPs have been shown to actively modulate cell function, and their presence in tissues has been assigned both pro- and anti-inflammatory roles (23).

Finally, redox signaling and low levels of H_2O_2 released by injured epithelial cells and tissue resident leukocytes are required for epithelial wound healing (24, 25), however H_2O_2 accumulation in inflamed tissue in the presence of MPO released by infiltrating PMNs may lead to oxidative stress and promote epithelial injury. Thus, the current work explored the potential role for neutrophil MPO in epithelial wound healing. Our studies describe a novel mechanism of MPO delivery to IECs by PMN-derived MPs under the condition of inflammation and its role in the regulation of IEC proliferation and migration during wound healing.

MATERIALS AND METHODS

Cells

Human intestinal epithelial cells T84s [29] and Caco2 BBE [30] were grown in Dulbecco's modified Eagle's medium (DMEM)-F12 50:50, supplemented with 10% fetal calf serum (FCS), 1% L-glutamine, 1% antibiotics, 1% non-essential amino acids, and 1.5% HEPES buffer as previously described. Mouse intestinal epithelial cells CMT-93 were grown in Dulbecco's modified Eagle's medium (DMEM) with supplements as described above. PMNs were isolated from human blood obtained from healthy volunteers by density gradient centrifugation (26, 27) and handled according to protocols for the protection of human subjects, as approved by the Northwestern University Institutional Review Board. PMNs were used for experiments within 2 hours of isolation.

Reagents

DMEM, L-glutamine, penicillin/streptomycin, and non-essential amino-acids for cell growth media were obtained from Cellgro (Manassas, VA), FCS was obtained from Atlanta Biologicals (Atlanta, GA). N-formyl-l-methionyl-leucyl-l-phenylalanine (fMLF), phorbol-12-myristate-13-acetate (PMA), latrunculin B, hydrogen peroxide ABTS, and 2-acetamido-2- deoxy-a-D-galactopyranoside were purchased from Sigma-Aldrich (St. Louis, MO). MPO inhibitor, Myeloperoxidase Inhibitor-I (a benzoic acid hydrazide analog) was purchased from Abcam (Cambridge, MA).

Antibodies

FITC-conjugated anti-CD11b mAb, and FITC-conjugated IgG control mAbs were purchased from BD Biosciences (Franklin Lakes, NJ). Human TruStain FcX (Fc Receptor Blocking Solution) was purchased from Biolegend (San Diego, CA) o-Pro3-iodide was purchased from Invitrogen (Carlsbad, CA). A function inhibitory anti-CD11b/CD18 mAb (CBRM1/29) was purified in-house as previously described (47), MPO from Abcam (Cambridge, MA). HRP-conjugated anti-mouse and anti-rabbit IgGs from Jackson Immunoresearch (West Grove, PA).

Generation of PMN microparticles

Human PMN microparticles (MPs) were isolated from the supernatants of PMNs (2×10^7 cells) that were stimulated with fMLF (1μM in 200μl $HBSS^+$, 20 min at 37°C), PMA (200nM in 200μl $HBSS^+$, 20 min at 37°C) or a combination of latrunculin B (Lt-B, 1μM in 200μl $HBSS^+$, 5 min at 37°C) followed by fMLF (1μM in 200μl $HBSS^+$, 15 min at 37°). PMN supernatants following stimulation were cleared of cells and cellular debris using two-stage centrifugation (400xg followed by 3000xg spins, 10min) and then subjected to ultra-centrifugation at 100,000xg. Pelleted MPs were washed and prepared for western blot analysis, flow cytometry or functional assays as described (28). For all functional assays MPs derived from 3×10^6 PMNs were used. *For preparation of murine* PMN microparticles, PMNs were isolated from bone marrow and enriched to ~85–90% purity using histopaque gradients (1077 and 1119, Sigma) as previously described (29). Murine PMNs (2×10^7 cells) were then stimulated with latrunculin B (Lt-B, 1μM in 200μl $HBSS^+$, 5 min at 37°) followed

by fMLF (5μM in 200μl $HBSS^+$, 15 min at 37°) and prepared using centrifugation methods as described above. Enzymatic activity of MPO in cell lysates, supernatants and associated with PMN-MPs (both human and mouse) was assessed using 2,2'-azino-bis-3-ethylbenzthiazoline-6-sulphonic acid (ABTS) as the substrate in the presence of H_2O_2 (30).

Flow cytometry

Total MPO expression was examined following fixation and permeabilization using BD Cytofix/Cytoperm kit (BD Biosciences, San Jose, CA) according to the manufacturer instructions. To assess surface expression of MPO, freshly isolated PMNs prior to or following stimulation were fixed and prepared for flow cytometry as previously described (31). To determine surface protein expression on human and mouse MPs, MPs were incubated with fluorescently conjugated antibodies or relevant isotype controls for 40 minutes on ice. All cell samples were analyzed using BD FACSCANTO II and FlowJo software.

Western Blot

PMNs before and following stimulation were lysed in 1% SDS buffer (with 100mM Tris pH 7.4) containing protease and phosphatase inhibitors (Sigma), boiled, and cleared by centrifugation. Equal amounts of protein from cell lysates (determined using a BCA protein assay) or from concentrated supernatants (normalized by volume) or PMN-MPs (derived from 3×10^6 PMNs unless otherwise specified) were separated by SDS-PAGE and transferred onto nitrocellulose membranes. Membranes were blocked for 1h with 5% non-fat milk in 0.05% Tween-20 Tris-buffered saline, and incubated with appropriate primary antibodies overnight at 4°C, followed by secondary HRP-conjugated antibodies. For protein analysis in cell supernatants equal protein loading was confirmed using Ponceau staining.

Immunofluorescence (IF) labeling

IEC monolayers grown on permeable supports or coverslips before and after the indicated treatment were ethanol fixed, blocked with 5% BSA in PBS and incubated with the relevant primary Ab (10μg/ml, over night at 4°C) either directly conjugated or followed by an appropriate fluorescently-labeled secondary antibody (1 hour at RT). For mouse tissue, punch biopsies (2mm diameter) of mucosal wounds and the corresponding non-wounded regions were frozen in OCT, cryo-sectioned (8μm width), and fixed/permeabilized with 3.7% paraformaldehyde and 2% triton in PBS as previously described (32). All images were captured using a Nikon A1R+ confocal microscope with 60X oil objective.

Cell adhesion assays

For PMNs, BCECF-labeled PMNs (1×10^6) were added to IECs (grown to confluence in 12-well plates) with or without the addition of fMLF (100nM) and function inhibitory anti-CD11b/CD18 mAb (CBRM1/29, 10 μg/ml). Epithelial monolayers were centrifuged at 50×g for 5 minutes to uniformly settle PMNs. Following 1 hour at 37°C, IEC monolayers and the adherent PMNs were gently washed with Hanks buffer, lysed and fluorescence intensity was measured. Adherent PMN numbers were determined from standard curves generated by serial dilution of known numbers of BCECF-AM–labeled PMNs. *For IECs*, single cell

suspensions were generated using a non-enzymatic cell dissociation buffer (Gibco). IECs (150000 cells/condition) were resuspended in 0.1 ml Hanks solution containing Mg2+, Ca2+ and 0.1% BSA, labeled with BCECF-AM (Invitrogen) and allowed to adhere to Matrigel™ (356234, BD) coated (overnight, 10μg/ml) BSA blocked 96 well plates for 1 hour at 37°C. Fluorescence intensity of cells that remained attached to the matrix after 3 consecutive washes was measured. All fluorescence measures were done using FluoStar Galaxy plate reader at excitation/emission wavelengths of 485/535 nm.

Wound-healing assays

For in vitro scratch-wound assays IEC monolayers were grown to confluence in 24-well tissue culture plates. A linear mechanical scratch wound was generated in each well using a 20μl plastic pipette tip attached to low suction (5). Wounded monolayers were washed once with PBS to remove detached cells and debris, and incubated in medium containing the appropriate treatment. The rate of cell migration into scratch wounds was measured by determining the surface area devoid of epithelial cells immediately after wounding (t = 0) and at subsequent time points as indicated. Where indicated, PMNs were added to scratch-wounded IEC monolayers at 1 PMN to 1 IEC ratio (5×10^6 cells). However, we established that ~50% of PMNs became adherent to IECs under these conditions, thus resulting in1:2 adherent PMNs to IECs ratio. The data are shown as percent area at each time point as indicated out of total area at t = 0. All experiments were carried out in triplicate, with at least an N = 3. Real-time videomicroscopy on scratch wounded IEC monolayers was done with an inverted phase contrast microscope (Leica) equipped with a temperature and CO_2 controlled chamber (5%CO2 at 37°C). DIC images were taken every 2 minutes for 4 hours and cell migratory patterns were analyzed of line using ImageJ software. *For in-vivo assays*, a colonoscopic-biopsy-wound model was used as previously described (32). Briefly, mechanical wounds in mouse colons (2–3 sites along the dorsal aspect) were generated using biopsy forceps and a high-resolution colonoscope (Coloview Veterinary Endoscope, Karl Stortz) in anesthetized (ketamine 100mg/kg and xylazine 5mg/kg) mice. The size of inflicted wounds was measured at days 1 and 4 post-wounding. At indicated intervals, mucosal wounds were harvested and prepared for immunofluorescence analysis. When indicated at day 1 (24 hours post-wounding) PMN-MPs were injected directly into the wound area using a colonoscopy-based microinjection technique.

Proliferation

To examine the effect of MPO on cell proliferation, cell cycle analyses and 5-ethyl-2`-deoxyuridine (EdU) incorporation assays were performed. For cell cycle analyses, cells were fixed in 70% ethanol (1hr, 4°C), treated with RNaseA (50μg/ml, 1 hr, 37°C), and stained with propidium iodide (25μg/ml, 30 min, 37°C). Samples were analyzed using an LSR II flow cytometer (BD Biosciences), and distribution of cell-cycle phases was determined using FlowJo software analysis. For EdU incorporation assay a Click-iT EdU Alexa 488 cell proliferation kit (Invitrogen) was used according to the manufacturer's instructions. *For in-vivo analysis* colonic cryo-sections were stained for the proliferation marker, Ki67.

Transmission electron microscopy

PMN-MPs were resuspended in PBS, fixed by adding equal volume of 2% PFA in 0.1 phosphate buffer (pH 7.4) to final volume of 100μl and absorbed onto 400-mesh carbon-coated copper grids (10 minutes). Imaging was performed using the FEI Tecnai Spirit G2 transmission electron microscope (28).

Statistics

Statistical significance was assessed by a Student t-test or by one-way ANOVA with a Newman-Keuls Multiple Comparison Test using Graphpad Prism (V4.0). Statistical significance was set at $p<0.05$.

RESULTS

PMNs induce MPO-dependent inhibition of IEC wound healing

Tissue infiltration by PMNs and generation of reactive oxygen species (ROS) can lead to tissue injury. We thus asked whether PMN interactions with wounded IECs could impair wound closure, and whether these effects would be dependent on MPO, which can generate ROS, such as hypochlorous acid (HOCl) (16). In these experiments, freshly isolated human PMNs (5×10^5) were added to scratch wounded Caco-2 BBe IEC monolayers (in the presence of 100nM fMLF to induce PMN adhesion, resulting in ~1 adherent PMN to 2 IECs) immediately following wounding. Subsequently, IEC wound closure was quantified at 24 and 48 hours with or without inhibition of MPO. PMN adhesion to IECs resulted in significant inhibition of wound closure, at both time points (Fig 1A and representative images, B). This inhibition was significantly attenuated in the presence of specific MPO inhibitor (MPO Inhibitor I, an analog of benzoic acid hydrazyde, 1μg/ml), suggesting a role for MPO in impaired IEC healing responses. The MPO-dependent inhibitory effect of PMNs on IEC wound closure was confirmed in an additional human IEC line, T84 (not shown). To further confirm the specificity of the observed inhibitory effects to MPO activity, wound closure of murine EICs (CMT-93) was examined in the presence of WT and MPO-KO murine PMNs. Both WT and MPO-KO PMNs inhibited CMT-93 cell wound healing, however, the effect of MPO-KO PMNs was significantly reduced compared to that of WT PMNs (Fig 1C). While a high concentration of fMLF (500nM) has been shown to affect IEC wound healing responses (33), in our studies lower concentration of fMLF (100nM) was sufficient to induce PMN activation and adhesion without affecting IEC restitution (Fig 1Sa).

Wounded IECs and PMNs can produce H_2O_2 (25), which serves as a substrate for PMN-MPO to generate toxic oxidants that could impair healing. Thus, to simulate tissue inflammation and PMN accumulation, and to confirm the role of MPO in IEC wound healing, scratch wound assays (using Caco2 BBe and T84 IECs) were conducted in the presence of recombinant MPO with and without the addition of exogenous H_2O_2. Consistent with PMN effects, treatment with recombinant MPO (1μg/ml) in combination with H_2O_2 (100μM) significantly delayed IEC wound closure both 24 and 48 hours post wounding (Fig 1D). Interestingly, MPO treatment alone had a small (not significant) effect on wound closure 24 hours post-wounding, however, the effect of MPO became significant at 48 hours,

consistent with the idea of H_2O_2 generation by wounded IECs and its overtime accumulation at the wound bed. With or without the addition of H_2O_2, inhibition of MPO activity restored IEC healing responses. At the selected concentration H_2O_2 had no effect on viability of IECs (confirmed by tunnel/PI and Annexin V staining for cell death and apoptosis respectively, not shown).

Alterations in the actin cytoskeleton facilitate MPO release by activated PMNs

Given the effect of MPO on IEC wound healing we examined cell surface localization and changes in total levels of MPO on activated PMNs. Disruption of the actin cytoskeleton, which can simulate PMN adhesion and spreading on IECs has been previously shown to induce MPO release by PMNs (34). Thus, flow cytometric analyses were performed on non-permeabilized (surface expression) and permeabilized (total expression) PMNs following stimulation with commonly used PMN activators; fMLF and PMA with or without pretreatment with actin-disrupting agent, Latrunculin B (Lt-B, 1μM). fMLF stimulation of PMNs with concentrations ranging from 100nM to 5μM (20min, 37°C) had no significant effect on MPO expression (5μM treatment shown in Fig 2A,B). A modest decrease in total MPO levels was seen following PMA treatment (200nM, 20min 37°C), however, interestingly, a significant mobilization of MPO to PMN surface was observed. Importantly, sequential PMN treatment with Lt-B, which has been used to experimentally disrupt the actin cytoskeleton (1μM, 5min, 37°C, (35, 36)), followed by fMLF (5μM, 20 min, 37°C, Lt-B/fMLF) or PMA (200 nM, not shown), while increased MPO expression at the cell surface, resulted in significantly decreased total MPO levels (Fig 2A,B), suggesting its release into the extracellular space. Representative images in Figure 2C show MPO surface expression and total levels following Lt-B/fMLF treatment compared to control conditions.

Alterations in the actin cytoskeleton are required for the release of PMN-MP associated MPO

To further define conditions of MPO release by PMNs, MPO expression was examined by immunoblotting of PMN lysates, cell supernatants and PMN-MPs, which have been shown to carry active effector enzymes and to modulate cellular function (28, 37). PMN stimulation with Lt-B/fMLF, but not fMLF alone or PMA resulted in decreased MPO levels in PMN lysates and appearance of MPO in PMN supernatants (Fig 3A). Importantly, an abundance of secreted MPO under these activating conditions was found to be associated with PMN-MPs (Fig 3A). MPO association with PMN-MPs was further confirmed by flow cytometry, where PMN-MPs were compared to 1μm beads (using flow cytometer forward and side scatter). PMN-MPs were defined as particles smaller than 1μm in diameter and that stained positive for phosphatidylserine, using Annexin V (commonly used to identify membrane derived particles (38) (Fig 3B). Representative images of a PMN-MPs (~600nm in diameter) are shown in electron microscopy micrographs (Fig 3C). Given the previously suggested role for MMP-9 and Annexin A1 (AnxA1) in PMN-mediated tissue injury and healing, respectively (32, 37), we also examined association of these proteins with MPs under aforementioned stimulating conditions. While fMLF and PMA stimulation of PMNs leads to enrichment of both pro- and anti-inflammatory MMP-9 and AnxA1 on MPs (respectively), intriguingly, association of these molecules with PMN-MPs following LtB/fMLF

stimulation was decreased (Fig 1Sb), suggesting stimulus dependent specificity of PMN-MP content.

Next we thought to determine whether MPO associated with PMN-MPs is enzymatically active. In these experiments, PMN-MPs isolated from 1, 3 and 5×10^6 PMNs following stimulation with Lt-B/fMLF were examined for peroxidase activity using 2,2'-azino-bis-3-ethylbenzthiazoline-6-sulphonic acid (ABTS) as a substrate in the presence of H_2O_2. Increased enzymatic activity was observed with increasing numbers of PMN-MPs, suggesting presence of active MPO on PMN-MPs (Fig 3D). Consistent with immunoblotting data, very low peroxidase activity was detected in supernatants from fMLF or PMA stimulated PMNs (1×10^6 PMN/condition), however this was significantly increased with Lt-B/fMLF treatment (Fig 3E). Importantly, PMN-MP release with active MPO was observed only following Lt-B/fMLF treatment (Fig 3E). These data demonstrate that activated PMNs can release MPs carrying active MPO to potentially modulate tissue function.

PMN adhesion to IECs triggers the release of soluble and MP-associated MPO

Disruption of the actin cytoskeleton facilitated the release of PMN-MPs rich in MPO (Fig 3). Since rapid reorganization of the actin cytoskeleton is required for PMN adhesion and polarization (39), we hypothesized that PMN adhesion to IECs may similarly result in release of PMN-MPs carrying active MPO, and that secreted PMN-MPs would be able to bind to the IEC surface and affect IEC wound healing. To test this idea, 1×10^6 PMNs were introduced to IECs (grown in 12-well tissue culture plates) and allowed to adhere for 3 hours at 37°C in the presence or absence of a low concentration of fMLF (100nM, to induce PMN adhesion) and/or PMN adhesion inhibitory anti-CD11b antibody (Ab) (10μg/ml, (10)). Low PMN adhesion to unstimulated IECs was significantly potentiated in the presence of fMLF, and was reversed with the addition of an anti-CD11b inhibitory Abs (Fig 4A). Consistent with our hypothesis and the observed MPO-dependent inhibition of IEC wound healing, fMLF-induced PMN adhesion to IECs resulted in MPO release both into the supernatants (soluble MPO, Fig 4B) and in association with PMN-MPs (Fig 4C). Since MPO release could be triggered by PMN apoptosis, we confirmed that at this time point no PMN apoptosis was observed (not shown). In support of the enzymatic assays, immunoblotting analysis of PMN-MPs isolated from supernatants of PMN and IEC co-cultures revealed an abundance of MPO (Fig 4D). The release of soluble and MP-bound MPO was significantly attenuated in the presence of PMN adhesion inhibitory anti-CD11b Abs, suggesting a contact-dependent effect. Furthermore, immunofluorescence analysis of IEC monolayers following co-culture with PMNs (red) in the presence of fMLF revealed a robust attachment of MPO positive aggregates (green) consistent with the size of PMN-MPs (> 1μm, (38)) (Fig 4E). Together these observations suggest that PMN adhesion to IECs can trigger the release of PMN-MPs, and that PMN-MPs can bind to the IEC surface to potentially mediate inhibitory effects on IEC wound healing.

PMN-MPs mediate MPO-dependent inhibition of IEC wound healing

To establish whether PMN-MP secretion could serve as a novel mechanism for PMN-mediated inhibition of IEC wound healing (Fig 1), we next examined the effect of PMN-MP binding (derived from LtB/fMLF-stimulated 3×10^6 PMNs) to IECs on IEC wound closure.

Consistent with effects of freshly isolated PMNs, PMN-MP treatment significantly inhibited IEC wound closure both 24 and 48 hours post-wounding (Fig 5A). PMN-MP inhibitory effects on IEC wound healing were further potentiated with the addition of exogenous H_2O_2. For both treatments, pharmacological inhibition of MPO activity reversed the observed effects, suggesting a specific role for PMN-MP associated MPO. Importantly, the effect of MP-MPO on IEC wound healing was examined in an additional model simulating physiological conditions, where MPs rich in active MPO were isolated from cell supernatants following PMN adhesion to confluent IECs (as shown in Fig 4). Consistent with the effect of MPs isolated from LtB/fMLF-stimulated PMNs, PMN adhesion-induced MPs in the presence of exogenous H_2O_2 inhibited IECs wound healing (Fig 5B). Under these conditions MP inhibitory effects on wound healing were also MPO-dependent, and were attenuated with the addition of MPO inhibitor. Since MPs isolated from PMN-IEC co-cultures may contain IEC-derived MPs in control experiments, the effect of MPs isolated from IECs alone without PMN adhesion on IEC wound healing was examined. No significant changes were observed (Fig 5B). To begin dissecting the mechanism for the MPO-dependent inhibition of wound healing, we next performed time-lapse imaging analyses to track the displacement of the leading edge cells under the specified conditions. We observed that the migratory capacity of leading cells at the wound edge was significantly decreased following treatments with PMN-MPs or recombinant MPO in the presence of H_2O_2 (Fig 5C and representative images with outlined cell displacement tracks D). In both cases decreased displacement of leading edge cells was rescued with the inhibition of MPO.

MPO inhibits IEC spreading and migration by interfering with actin dynamics

IEC attachment and spreading are critical for efficient migration of the epithelial sheet. To gain further insight into the mechanistic effects of MPO on IEC wound healing we analyzed the effect of both recombinant and PMN-MP associated MPO on IEC attachment and spreading. First we examined the effect of MPO with/without the addition of H_2O_2 on integrin-mediated IEC attachment to collagen-coated surfaces. No significant effects were observed with either the recombinant or PMN-MP associated MPO (Fig 6A), arguing intact integrin function. We next examined the effect of MPO treatment on IEC spreading. As shown in representative images (Fig 6B) and quantified in Figure 6C, treatment with recombinant MPO and PMN-MPs in the presence of H_2O_2 significantly inhibited spreading of subconfluent IECs. Consistent with the role of MPO in this process, the addition of MPO inhibitor restored the spreading ability of IECs.

Changes in cell shape during spreading and forward movement of the epithelial sheet require active reorganization of the actin cytoskeleton (7) and extension of membrane protrusions (lamellipodia) (8). Thus, we next examined the effect of recombinant MPO and PMN-MPs on the ability of migrating leading edge cells to extend lamellipodia, and on the organization of actin filaments by leading edge cells. Supporting previous findings (5) prominent lamellipodia formation was seen in control IECs (Fig 7A and B), however, this process was significantly attenuated in the presence of recombinant MPO and PMN-MPs. For both treatments, inhibition of lamellipodia formation was further potentiated by the addition of exogenous H_2O_2, consistent with the idea of cumulative endogenous (IEC-derived) and exogenous (PMN-derived) H_2O_2 contributions to the impairment of wound healing

responses in the presence of MPO. Inhibition of MPO activity reversed these effects (Fig 7A). Furthermore, impaired actin fiber organization (zoom-in images, Fig 7B) and significant actin accumulation at the leading edge of migrating IECs following treatment with MPO/PMN-MP and H_2O_2 was observed (Fig 7C), indicating impaired actin dynamics (24).

Recombinant and PMN-MP associated MPO inhibits IEC proliferation by inducing cell cycle arrest

In addition to migration, cell proliferation is an important contributor to epithelial wound healing (32). Thus, we investigated the effect of PMN-MPs/MPO on IEC proliferation. Cell cycle analysis of subconfluent IECs following treatment with recombinant MPO and PMN-MP associated MPO (using Propidium Iodide staining and flow cytometry) in the presence of H_2O_2 revealed a significant accumulation of IECs in G2/M phase (from 10.2±1.3%, control to 43.2±2.8% and 49.3±2.9%, recombinant and PMN-MP MPO respectively) indicating cell cycle arrest (Fig 8A). These observations were further corroborated using Edu incorporation assay in scratch wounded IECs. The number of proliferating IECs at the wound edge was significantly decreased following treatment with either recombinant MPO or PMN-MPs, in the presence of H_2O_2 (Fig 8B and representative images, Fig 8C). The addition of MPO inhibitors attenuated these effects, confirming the role of MPO in these responses. Together these findings suggest that the release of PMN-MPs and the activity of MPO by wound-infiltrating PMNs dampen IEC wound healing responses by downregulating actin dynamics and inhibiting cellular migration and proliferation.

PMN-MPs mediate MPO-dependent inhibition of IEC proliferation and wound healing *in vivo*

We next thought to examine the role for PMN-MPs and MPO *in vivo*. To this purpose we first isolated MPs from WT and MPO knockout bone marrow-derived PMNs (WT PMN-MPs and KO PMN-MPs, respectively) following sequential stimulation with Lt-B (1μM, 5min 37°C) and fMLF (5μM, 20min, 37°C). Immunoblotting and enzymatic analysis confirmed MPO presence and peroxidase activity for WT PMN-MPs, but not KO PMN-MPs (Fig 9A and B). Next, the inhibitory potential of WT PMN-MPs and control KO PMN-MPs was examined in scratch wound assays using murine IECs (CMT-93). The addition of WT PMN-MPs to scratch-wounded murine IECs resulted in significant inhibition of wound closure. This effect was further potentiated with the addition of the MPO substrate, H_2O_2 (Fig 9C), and reversed with MPO inhibitor. Importantly, treatment with KO PMN-MPs failed to inhibit IEC wound healing, arguing an MPO-specific effect (Fig 9C). Consistent with observations in human cell lines, MPO-dependent inhibition of IEC proliferation was observed (Fig 9D). Finally, we utilized a colonic-mucosal, biopsy-based wound model (32, 38) to examine the effect of PMN-MPs and MPO *in vivo*. In this setup, superficial mucosal wounds were introduced to mouse colons, and wound healing was monitored for 4 days post-wounding using endoscopic imaging. When indicated, WT or KO PMN-MPs were microinjected directly into the wound area 24hr post-wounding (Fig 9G, (32)). WT PMN-MPs induced ~2-fold decrease in wound closure compared to control wounds (Fig 9E and representative images, Fig 9F). No significant effect on mucosal wound healing was observed with injection of KO PMN-MPs, confirming a role for PMN-MPs and MPO in

wound healing *in vivo*. Inhibition of wound healing mediated by WT PMN-MP was due to decreased IEC proliferation (Fig 9H and representative images of Ki67 staining Fig 9I, lower panels) and delayed re-epithelialization of the colonic mucosa (Fig 9I, upper panels), as evident from immunofluorescence labeling of frozen tissue sections from colonic mucosal wounds (day 4 after wounding).

DISCUSSION

Dysregulated PMN recruitment as seen in IBD is often associated with cell death and tissue injury (9). Activated PMNs can induce tissue damage via several mechanisms including the release proteolytic enzymes and the production of ROS (40, 41). As such, activated PMNs are known to generate H_2O_2, which is catalyzed by the heme enzyme, MPO (most abundantly expressed protein in PMNs), to form a potent oxidant, hypochlorous acid (HOCl) (16). Pathological effects of MPO and HOCl on vascular endothelial cells and the underlying tissue function have been demonstrated in numerous diseases, including coronary artery disease and atherosclerosis(42). In epithelial cells, MPO activity has been shown to induce DNA damage (43) and to correlate with IBD pathology (20). Thus, in the current work we thought to investigate the effect of MPO on IEC wound healing. We found that alterations in the actin cytoskeleton (chemically-induced or following PMN adhesion to IECs) significantly potentiated activation-induced release of MPO by PMNs. MPO was secreted in a soluble form as well as in association with PMN-derived MPs and was found to mediate potent inhibition of IEC migration and proliferation leading to delayed wound healing. Consistent with previous work (44), we found that PMN stimulation with fMLF or PMA resulted in low-level MPO release, however, the release of MPO was significantly increased when the cytoskeleton-disrupting agent, latrunculin B (Lt-B) was used prior to PMN stimulation. Interestingly, PMA but not fMLF treatment triggered a significant mobilization of MPO to the cell surface. The role of MPO at the PMN cell surface is not clear yet, however, our observation supports other work that found increased surface MPO expression on PMNs in pregnant mice (45). High surface MPO expression in these mice was suggested to compensate for the PMNs inability to mount efficient oxidative responses. Another possibility for the increased surface levels of MPO is the ability of released MPO to bind back to CD11b (a β_2-integrin expressed at the PMN surface) to induce CD11b-dependent signaling in PMNs (46). Given the important role for CD11b in PMN trafficking (10, 47) it is possible that extracellular MPO may contribute to the regulation of PMN recruitment.

Release of MPs has recently emerged as an important mechanism for PMNs to locally modulate tissue function and immune responses. Intriguingly, PMN-MPs were assigned both anti- and pro-inflammatory functions in various tissues. For example, MPs released into circulation by activated PMNs were found to competitively inhibit PMN adhesion and extravasation, thus potentially limiting the inflammatory response (48). Likewise, MPs secreted by tissue infiltrating PMNs were found to penetrate arthritic joints and protect against cartilage degeneration by annexin A1-dependent action (37). In contrast, in response to external stimuli, PMN-MPs were found to generate ROS or produce leukotriene B4 (21), which could potentiate tissue injury. Furthermore, PMN-MPs mediated MPO-dependent barrier disruption in endothelial cells (49). The yin and yang of PMN-MP function may

result from size heterogeneity, variations in protein composition and expression levels, and may depend on specific stimulating conditions. Indeed, we found fMLF or PMA simulation of PMNs results in the release of MMP-9 rich MPs (28), TNFα stimulation increased AnxA1 expression, however, MPO enrichment on MPs was restricted to Lt-B/fMLF treatment. Given stimulus dependence, MP protein composition may vary if released following PMN adhesion or migration across endothelial/epithelial layers or PMN tissue migration. Thus, while adhesion-induced MPs can carry high levels of an anti-inflammatory AnxA1 to mediate inhibition of PMN-endothelial cell interactions (48), MPs released by transmigrating PMNs may contain MPO to mediate endothelial damage. Similarly, MPs released by tissue navigating PMNs may also be rich in AnxA1 and mediate protective effects (37).

Finally, PMN-MP size (which, may also influence protein composition and tissue accessibility) and content are likely to be coupled to PMN degranulation, thus increased understanding of mechanisms involved in PMN-MPs release may aid in the future to establish conditions for anti- versus pro-inflammatory function of PMN-MPs.

We recently demonstrated that the shedding of junctional adhesion molecule like protein (JAML) by activated PMNs and JAML binding to coxsackievirus and adenovirus receptor (CAR) resulted in inhibition of IEC wound healing (31). Neutralizing JAML-CAR interactions only partially recovered restitutive responses, suggesting that additional PMN-derived mediators may be involved in this process. In the current work, we show MPO/products of MPO enzymatic activity can similarly inhibit IEC wound healing. Importantly, we show for the first time that unlike JAML which was excluded from PMN-MPs, MPO was mobilized and secreted in association with PMN-MPs to exhibit potent inhibition of IEC wound healing. Moreover, PMN-MP MPO was more effective in mediating inhibitory effects on IEC wound healing compared to recombinant MPO at similar concentrations (1μg/ml). This could be due to a more direct and localized MPO delivery to IECs by PMN-MPs, and/or increased MPO stability when bound to lipid bi-layers compared to soluble MPO. Indeed, MPO binding to HDL in cardiovascular disease has been shown to protect MPO from cellular uptake and degradation (50). Whether this is true for PMN-MPs should be determined in future studies. In addition, other proteins or oxidative agents that may associate with PMN-MPs under these conditions could provide additive effects to that of MPO in inhibition of wound healing.

Finally, we show that both cellular migration and proliferation were affected by the MPO activity. Cell tracking microscopy revealed impaired ability of IECs to spread and exhibit efficient forward movement in the presence of recombinant and PMN-MP associated MPO and H_2O_2. As such, following both treatments, migrating IECs were unable to form leading edge lamellipodia that serve as footholds to propel the cell forward.

Similarly, while control IECs showed organized actin fibers and dispersal of actin within the lamellipodia, treatment with recombinant and PMN-MP associated MPO combined with H_2O_2 showed impaired actin fiber formation by migrating IECs and significant accumulation of F-actin at the leading edge.

In summary, our findings suggest that PMN MPO may promote PMN-induced intestinal epithelial injury by inhibiting restitutive responses. Furthermore, our work implicates MPs secreted by tissue infiltrating PMNs as an efficient delivery system to locally modulate tissue function.

Supplementary Material

Refer to Web version on PubMed Central for supplementary material.

Acknowledgments

We thank Dr. Koch and the Northwestern University Center for Advanced Microscopy core (supported by NCI CCSG P30 CA060553 awarded to the Robert H Lurie Comprehensive Cancer Center) for the help with electron and confocal microscopy imaging of PMN-MPs.

Grant Support: This work was supported by grants from the National Institutes of Health (NIH) DK101675 as well as American Cancer Society IRG-9303718.

REFERENCES

1. Fasano A, Shea-Donohue T. Mechanisms of disease: the role of intestinal barrier function in the pathogenesis of gastrointestinal autoimmune diseases. Nature clinical practice. Gastroenterology & hepatology. 2005; 2:416–422.
2. Ma TY. Intestinal epithelial barrier dysfunction in Crohn's disease. Proceedings of the Society for Experimental Biology and Medicine. Society for Experimental Biology and Medicine. 1997; 214:318–327.
3. Maloy KJ, Powrie F. Intestinal homeostasis and its breakdown in inflammatory bowel disease. Nature. 2011; 474:298–306. [PubMed: 21677746]
4. Sturm A, Dignass AU. Epithelial restitution and wound healing in inflammatory bowel disease. World journal of gastroenterology : WJG. 2008; 14:348–353. [PubMed: 18200658]
5. Sumagin R, Robin AZ, Nusrat A, Parkos CA. Activation of PKCbetaII by PMA facilitates enhanced epithelial wound repair through increased cell spreading and migration. PloS one. 2013; 8:e55775. [PubMed: 23409039]
6. Cau J, Hall A. Cdc42 controls the polarity of the actin and microtubule cytoskeletons through two distinct signal transduction pathways. Journal of cell science. 2005; 118:2579–2587. [PubMed: 15928049]
7. Webb DJ, Parsons JT, Horwitz AF. Adhesion assembly, disassembly and turnover in migrating cells -- over and over and over again. Nature cell biology. 2002; 4:E97–E100. [PubMed: 11944043]
8. Small JV, Stradal T, Vignal E, Rottner K. The lamellipodium: where motility begins. Trends in cell biology. 2002; 12:112–120. [PubMed: 11859023]
9. Xavier RJ, Podolsky DK. Unravelling the pathogenesis of inflammatory bowel disease. Nature. 2007; 448:427–434. [PubMed: 17653185]
10. Sumagin R, Robin AZ, Nusrat A, Parkos CA. Transmigrated neutrophils in the intestinal lumen engage ICAM-1 to regulate the epithelial barrier and neutrophil recruitment. Mucosal immunology. 2014; 7:905–915. [PubMed: 24345805]
11. Langhorst J, Elsenbruch S, Mueller T, Rueffer A, Spahn G, Michalsen A, Dobos GJ. Comparison of 4 neutrophil-derived proteins in feces as indicators of disease activity in ulcerative colitis. Inflammatory bowel diseases. 2005; 11:1085–1091. [PubMed: 16306771]
12. Sumagin R, Parkos CA. Epithelial adhesion molecules and the regulation of intestinal homeostasis during neutrophil transepithelial migration. Tissue barriers. 2015; 3:e969100. [PubMed: 25838976]
13. Roman RM, Wendland AE, Polanczyk CA. Myeloperoxidase and coronary arterial disease: from research to clinical practice. Arquivos brasileiros de cardiologia. 2008; 91:e11–e19. [PubMed: 18660935]

14. Malle E, Furtmuller PG, Sattler W, Obinger C. Myeloperoxidase: a target for new drug development? British journal of pharmacology. 2007; 152:838–854. [PubMed: 17592500]
15. Odobasic D, Kitching AR, Semple TJ, Holdsworth SR. Endogenous myeloperoxidase promotes neutrophil-mediated renal injury, but attenuates T cell immunity inducing crescentic glomerulonephritis. Journal of the American Society of Nephrology : JASN. 2007; 18:760–770. [PubMed: 17267745]
16. Klebanoff SJ, Kettle AJ, Rosen H, Winterbourn CC, Nauseef WM. Myeloperoxidase: a front-line defender against phagocytosed microorganisms. Journal of leukocyte biology. 2013; 93:185–198. [PubMed: 23066164]
17. Malle E, Waeg G, Schreiber R, Grone EF, Sattler W, Grone HJ. Immunohistochemical evidence for the myeloperoxidase/H2O2/halide system in human atherosclerotic lesions: colocalization of myeloperoxidase and hypochlorite-modified proteins. European journal of biochemistry / FEBS. 2000; 267:4495–4503.
18. Reynolds WF, Rhees J, Maciejewski D, Paladino T, Sieburg H, Maki RA, Masliah E. Myeloperoxidase polymorphism is associated with gender specific risk for Alzheimer's disease. Experimental neurology. 1999; 155:31–41. [PubMed: 9918702]
19. Al Ghouleh I, Khoo NK, Knaus UG, Griendling KK, Touyz RM, Thannickal VJ, Barchowsky A, Nauseef WM, Kelley EE, Bauer PM, Darley-Usmar V, Shiva S, Cifuentes-Pagano E, Freeman BA, Gladwin MT, Pagano PJ. Oxidases and peroxidases in cardiovascular and lung disease: new concepts in reactive oxygen species signaling. Free radical biology & medicine. 2011; 51:1271–1288. [PubMed: 21722728]
20. Kim JJ, Shajib MS, Manocha MM, Khan WI. Investigating intestinal inflammation in DSS-induced model of IBD. Journal of visualized experiments : JoVE. 2012
21. Dalli J, Montero-Melendez T, Norling LV, Yin X, Hinds C, Haskard D, Mayr M, Perretti M. Heterogeneity in neutrophil microparticles reveals distinct proteome and functional properties. Molecular & cellular proteomics : MCP. 2013; 12:2205–2219. [PubMed: 23660474]
22. Tetta C, Ghigo E, Silengo L, Deregibus MC, Camussi G. Extracellular vesicles as an emerging mechanism of cell-to-cell communication. Endocrine. 2013; 44:11–19. [PubMed: 23203002]
23. Lo Cicero A, Stahl PD, Raposo G. Extracellular vesicles shuffling intercellular messages: for good or for bad. Current opinion in cell biology. 2015; 35:69–77. [PubMed: 26001269]
24. Matthews JD, Sumagin R, Hinrichs B, Nusrat A, Parkos CA, Neish AS. Redox control of Cas phosphorylation requires Abl kinase in regulation of intestinal epithelial cell spreading and migration. American journal of physiology. Gastrointestinal and liver physiology. 2016; 311:G458–G465. [PubMed: 27418680]
25. Suzuki N, Mittler R. Reactive oxygen species-dependent wound responses in animals and plants. Free radical biology & medicine. 2012; 53:2269–2276. [PubMed: 23085520]
26. Parkos CA, Colgan SP, Delp C, Arnaout MA, Madara JL. Neutrophil migration across a cultured epithelial monolayer elicits a biphasic resistance response representing sequential effects on transcellular and paracellular pathways. The Journal of cell biology. 1992; 117:757–764. [PubMed: 1577855]
27. Chin AC, Fournier B, Peatman EJ, Reaves TA, Lee WY, Parkos CA. CD47 and TLR-2 cross-talk regulates neutrophil transmigration. J Immunol. 2009; 183:5957–5963. [PubMed: 19812191]
28. Butin-Israeli V, Houser MC, Feng M, Thorp EB, Nusrat A, Parkos CA, Sumagin R. Deposition of microparticles by neutrophils onto inflamed epithelium: a new mechanism to disrupt epithelial intercellular adhesions and promote transepithelial migration. FASEB journal : official publication of the Federation of American Societies for Experimental Biology. 2016
29. Swamydas M, Lionakis MS. Isolation, purification and labeling of mouse bone marrow neutrophils for functional studies and adoptive transfer experiments. Journal of visualized experiments : JoVE. 2013:e50586. [PubMed: 23892876]
30. Venezie RD, Jenzano JW, Lundblad RL. Differentiation of myeloperoxidase and glandular peroxidase in biological fluids: application to human saliva. Journal of clinical laboratory analysis. 1991; 5:57–59. [PubMed: 1847970]
31. Weber DA, Sumagin R, McCall IC, Leoni G, Neumann PA, Andargachew R, Brazil JC, Medina-Contreras O, Denning TL, Nusrat A, Parkos CA. Neutrophil-derived JAML inhibits repair of

intestinal epithelial injury during acute inflammation. Mucosal immunology. 2014; 7:1221–1232. [PubMed: 24621992]

32. Sumagin R, Brazil JC, Nava P, Nishio H, Alam A, Luissint AC, Weber DA, Neish AS, Nusrat A, Parkos CA. Neutrophil interactions with epithelial-expressed ICAM-1 enhances intestinal mucosal wound healing. Mucosal immunology. 2016
33. Babbin BA, Jesaitis AJ, Ivanov AI, Kelly D, Laukoetter M, Nava P, Parkos CA, Nusrat A. Formyl peptide receptor-1 activation enhances intestinal epithelial cell restitution through phosphatidylinositol 3-kinase-dependent activation of Rac1 and Cdc42. Journal of immunology. 2007; 179:8112–8121.
34. Miyasaki KT, Song JP, Murthy RK. Secretion of myeloperoxidase isoforms by human neutrophils. Analytical biochemistry. 1991; 193:38–44. [PubMed: 1645935]
35. Bengtsson T, Orselius K, Wettero J. Role of the actin cytoskeleton during respiratory burst in chemoattractant-stimulated neutrophils. Cell biology international. 2006; 30:154–163. [PubMed: 16448823]
36. Sengupta K, Aranda-Espinoza H, Smith L, Janmey P, Hammer D. Spreading of neutrophils: from activation to migration. Biophysical journal. 2006; 91:4638–4648. [PubMed: 17012330]
37. Headland SE, Jones HR, Norling LV, Kim A, Souza PR, Corsiero E, Gil CD, Nerviani A, Dell'Accio F, Pitzalis C, Oliani SM, Jan LY, Perretti M. Neutrophil-derived microvesicles enter cartilage and protect the joint in inflammatory arthritis. Science translational medicine. 2015; 7 315ra190.
38. Leoni G, Neumann PA, Kamaly N, Quiros M, Nishio H, Jones HR, Sumagin R, Hilgarth RS, Alam A, Fredman G, Argyris I, Rijcken E, Kusters D, Reutelingsperger C, Perretti M, Parkos CA, Farokhzad OC, Neish AS, Nusrat A. Annexin A1-containing extracellular vesicles and polymeric nanoparticles promote epithelial wound repair. The Journal of clinical investigation. 2015; 125:1215–1227. [PubMed: 25664854]
39. Wong K, Pertz O, Hahn K, Bourne H. Neutrophil polarization: spatiotemporal dynamics of RhoA activity support a self-organizing mechanism. Proceedings of the National Academy of Sciences of the United States of America. 2006; 103:3639–3644. [PubMed: 16537448]
40. Brazil JC, Louis NA, Parkos CA. The role of polymorphonuclear leukocyte trafficking in the perpetuation of inflammation during inflammatory bowel disease. Inflammatory bowel diseases. 2013; 19:1556–1565. [PubMed: 23598816]
41. Fournier BM, Parkos CA. The role of neutrophils during intestinal inflammation. Mucosal immunology. 2012; 5:354–366. [PubMed: 22491176]
42. Nicholls SJ, Hazen SL. Myeloperoxidase and cardiovascular disease. Arteriosclerosis, thrombosis, and vascular biology. 2005; 25:1102–1111.
43. Gomez-Mejiba SE, Zhai Z, Gimenez MS, Ashby MT, Chilakapati J, Kitchin K, Mason RP, Ramirez DC. Myeloperoxidase-induced genomic DNA-centered radicals. The Journal of biological chemistry. 2010; 285:20062–20071. [PubMed: 20406811]
44. Dayer P, Leemann T, Kupfer A, Kronbach T, Meyer UA. Stereo- and regioselectivity of hepatic oxidation in man--effect of the debrisoquine/sparteine phenotype on bufuralol hydroxylation. European journal of clinical pharmacology. 1986; 31:313–318. [PubMed: 2878813]
45. Kindzelskii AL, Clark AJ, Espinoza J, Maeda N, Aratani Y, Romero R, Petty HR. Myeloperoxidase accumulates at the neutrophil surface and enhances cell metabolism and oxidant release during pregnancy. European journal of immunology. 2006; 36:1619–1628. [PubMed: 16688678]
46. Lau D, Mollnau H, Eiserich JP, Freeman BA, Daiber A, Gehling UM, Brummer J, Rudolph V, Munzel T, Heitzer T, Meinertz T, Baldus S. Myeloperoxidase mediates neutrophil activation by association with CD11b/CD18 integrins. Proceedings of the National Academy of Sciences of the United States of America. 2005; 102:431–436. [PubMed: 15625114]
47. Sumagin R, Prizant H, Lomakina E, Waugh RE, Sarelius IH. LFA-1 and Mac-1 define characteristically different intralumenal crawling and emigration patterns for monocytes and neutrophils in situ. Journal of immunology. 2010; 185:7057–7066.

48. Dalli J, Norling LV, Renshaw D, Cooper D, Leung KY, Perretti M. Annexin 1 mediates the rapid anti-inflammatory effects of neutrophil-derived microparticles. Blood. 2008; 112:2512–2519. [PubMed: 18594025]

49. Pitanga TN, Franca Lde Aragao, Rocha VC, Meirelles T, Borges VM, Goncalves MS, Pontes-de-Carvalho LC, Noronha-Dutra AA, dos-Santos WL. Neutrophil-derived microparticles induce myeloperoxidase-mediated damage of vascular endothelial cells. BMC cell biology. 2014; 15:21. [PubMed: 24915973]

50. Schindhelm RK, van der Zwan LP, Teerlink T, Scheffer PG. Myeloperoxidase: a useful biomarker for cardiovascular disease risk stratification? Clinical chemistry. 2009; 55:1462–1470. [PubMed: 19556446]

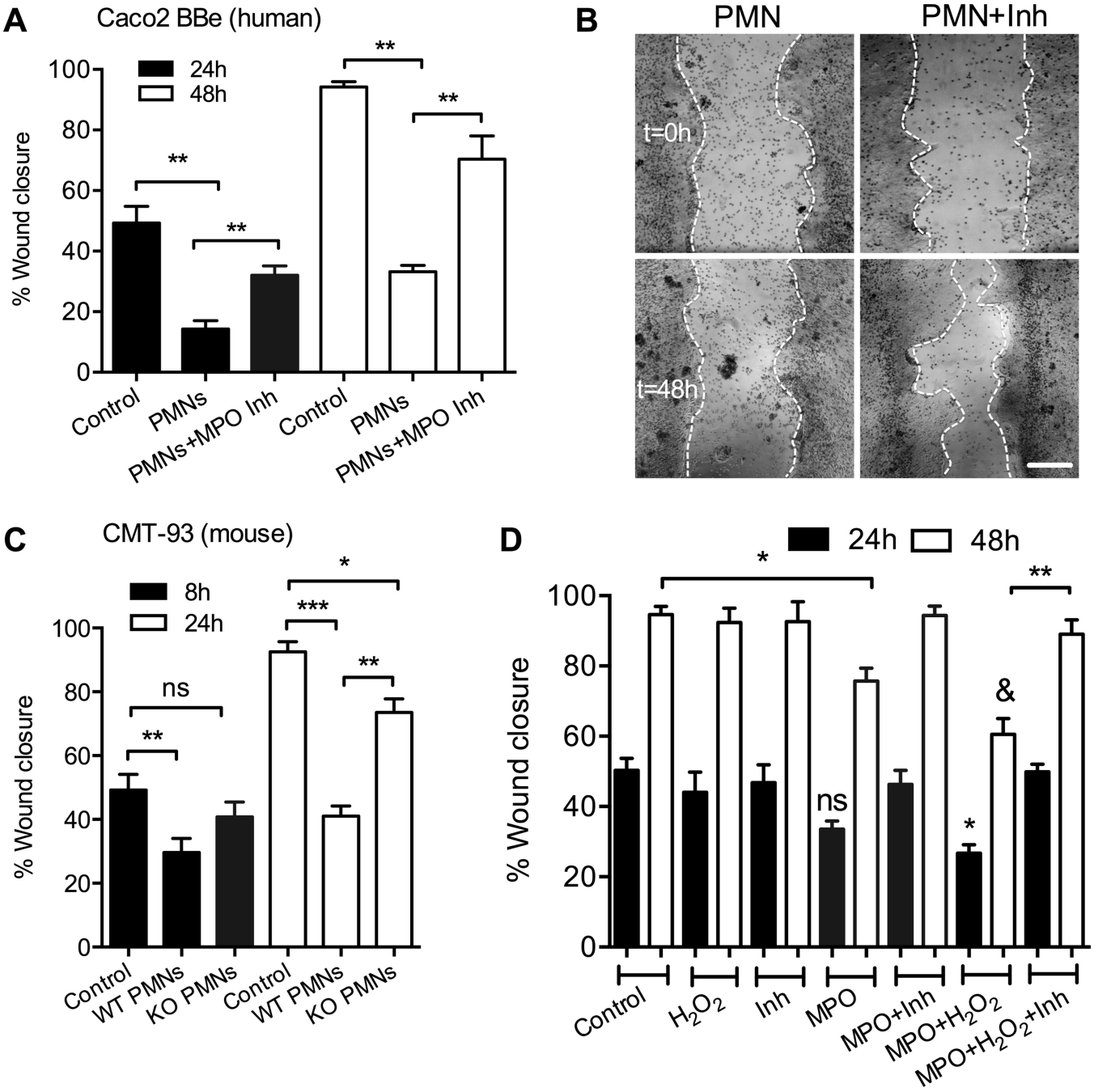

Figure 1. PMN adhesion to human IECs leads to MPO dependent inhibition of wound healing

(A) Scratch wound assays were performed to examine the effect of PMN adhesion and the release of MPO on wound closure of human IECs (Caco-2 BBe). PMN adhesion induced by fMLF (100nM, ratio of 1 adherent PMN to 2 IEC cells) significantly decreased wound closure. PMN inhibition of wound closure was significantly decreased in the presence of MPO inhibitor (MPO Inhibitor I, 1μg/ml). ** $p<0.01$. **(B)** Images representative of 4 independent experiments showing wounded monolayers that were incubated with PMNs with and without an MPO inhibitor immediately (t=0 upper panels) and 48 hours (lower

panels) post wounding. The bar is 100μm. (C) Scratch wound assays were conducted using murine EICs (CMT-93) in the presence of WT and MPO-KO murine PMNs to confirm the role for MPO in inhibition of wound healing. CMT wound healing was significantly reduced with the adhesion of MPO-KO compared WT PMNs. * $p<0.05$, ** $p<0.01$, *** $p<0.001$, ^{ns} not significant ($p>0.05$). **(D)** To confirm the specific role of MPO in IEC wound healing, scratch wound assays were performed in the presence of recombinant MPO (1μg/ml) with and without the addition of H_2O_2 and MPO inhibitor. MPO and H_2O_2 treatment significantly decreased IEC wound closure both 24 and 48 hours post wounding. ^{ns} not significant, * $p<0.05$, ** $p<0.01$. $^{\&}$ $p<0.01$ different from control. For A, C, and D data are presented as an average of 3 independent experiments.

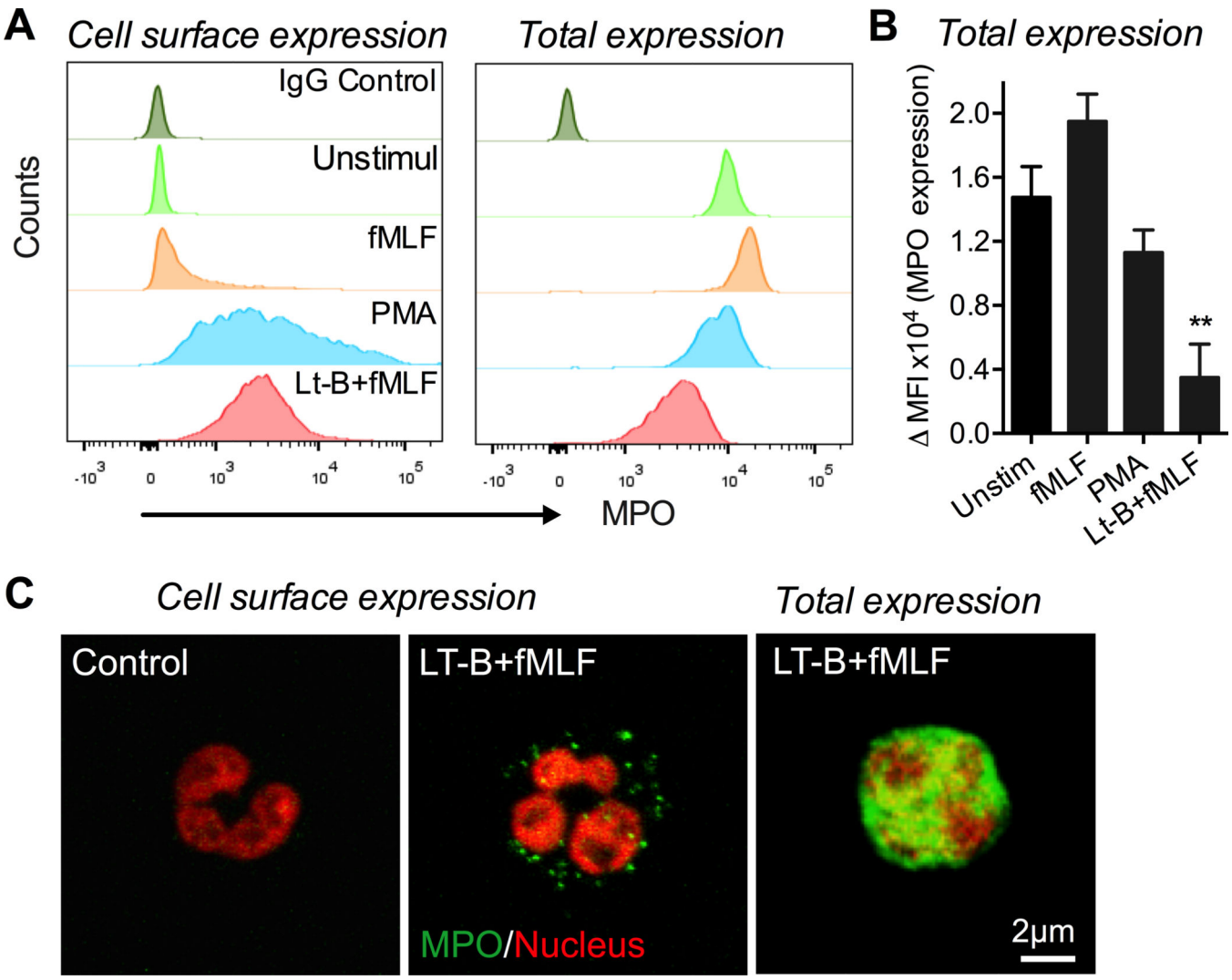

Figure 2. Alterations in actin cytoskeleton are required for the release of MPO by activated human PMNs

Freshly isolated PMNs were stimulated with fMLF (1μM, 20min, 37°C), PMA (200nM, 20min, 37°C) or a combination of Latrunculin B (Lt-B) (1μM, 5min), and fMLF (1μM, 15min, 37°C) in sequence. MPO cell surface and total expression on non-permeabilized and permeabilized PMNs respectively was analyzed. Latrunculin B was used to disrupt the PMN cytoskeleton, simulating PMN adhesion. **(A)** Representative flow micrographs (n=3) show mobilization of MPO to the cell surface following PMA and Lt-B/fMLF treatment, however, decreased total levels of MPO were observed only following Lt-B/fMLF treatment. **(B)** Quantification of changes in MPO expression as analyzed by flow cytometry. ** $p<0.01$. **(C)** Fluorescence staining of PMNs for cell surface expression of MPO (green) under the control condition (left panel) and the Lt-B/fMLF stimulation (middle panel). Total expression of MPO following Lt-B/fMLF treatment (right panel). Nuclei (red) were stained with cell permeable Vybrant Dye orange. The images are representatives of 3 independent experiments.

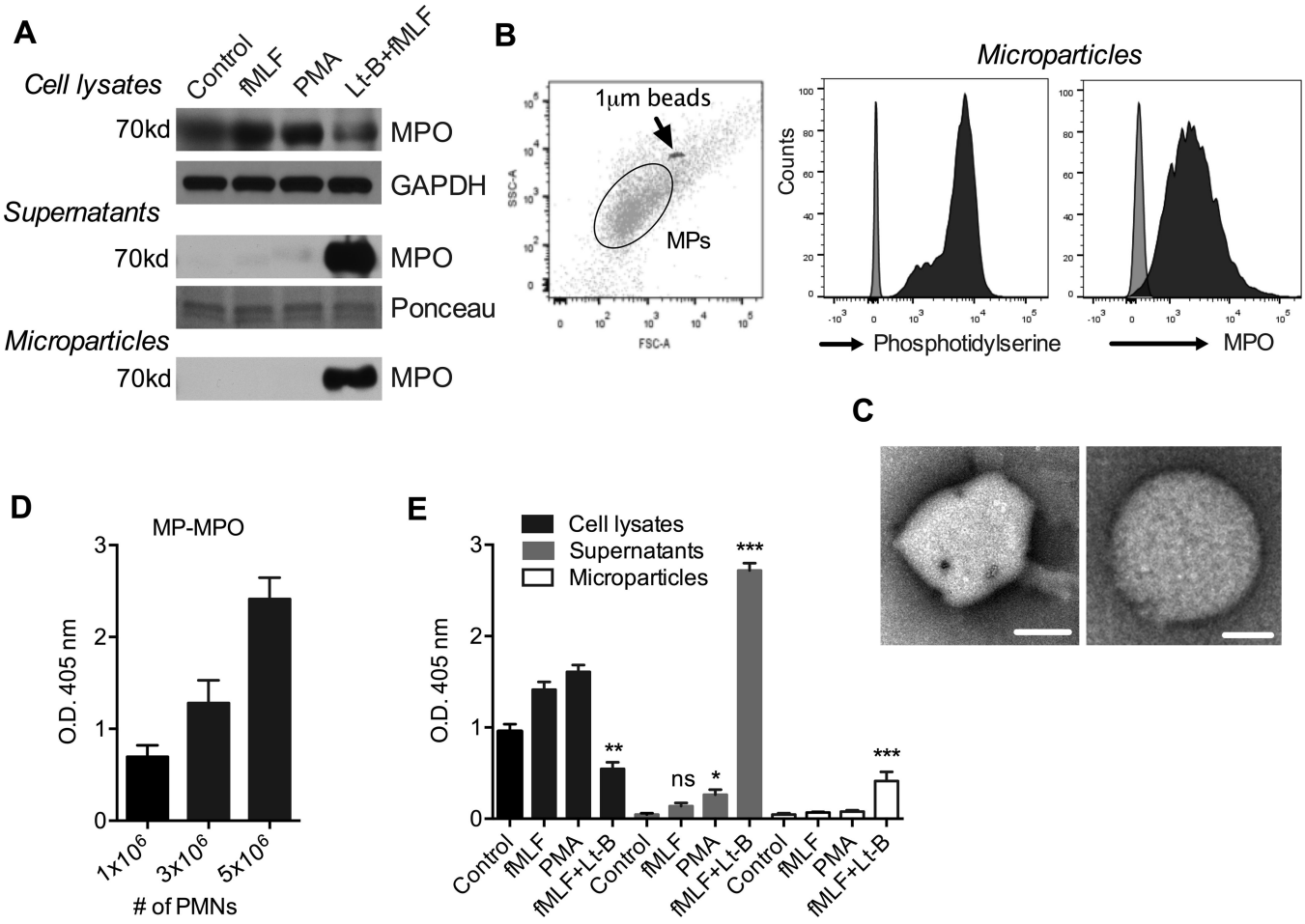

Figure 3. PMNs can release soluble and MP-associated MPO

(A) Expression of MPO under the specified activation conditions (1×10^6 PMN/treatment) was examined by immunoblotting of PMN cell lysates, supernatants and on PMN-MPs. Lt-B/fMLF stimulation resulted in decreased MPO levels in PMN lysates and appearance of MPO in cell supernatants and in association with PMN-MPs, consistent with its release by PMNs. Equal protein loading in cell supernatants was confirmed using Ponceau staining. **(B)** The presence of PMN-MPs, (particles smaller than 1μm) in supernatants of activated PMNs was confirmed by flow cytometry (left panel). PMN-MPs were further characterized by flow cytometry for the expression of membrane marker, Annexin V and MPO. **(C)** Transmission electron microscopy micrograph depicts a representative PMN-derived MP. Bars are 300nm and 150nm (left and right panels, respectively). For A, B, and C the images are representative of 3 independent experiments. **(D–E)** Assay for peroxidase activity using ABTS as the substrate was performed. **(D)** MPs derived from increasing numbers of Lt-B/fMLF stimulated PMNs exhibited higher MPO activity. **(E)** PMNs (1×10^6 PMN) were stimulated with fMLF, PMA or Lt-B/fMLF and MPO activity in cell lysates, supernatants and MPs was determined. * $p<0.05$, ** $p<0.01$, *** $p<0.01$ different from the appropriate control. ^{ns} not significantly different from control.

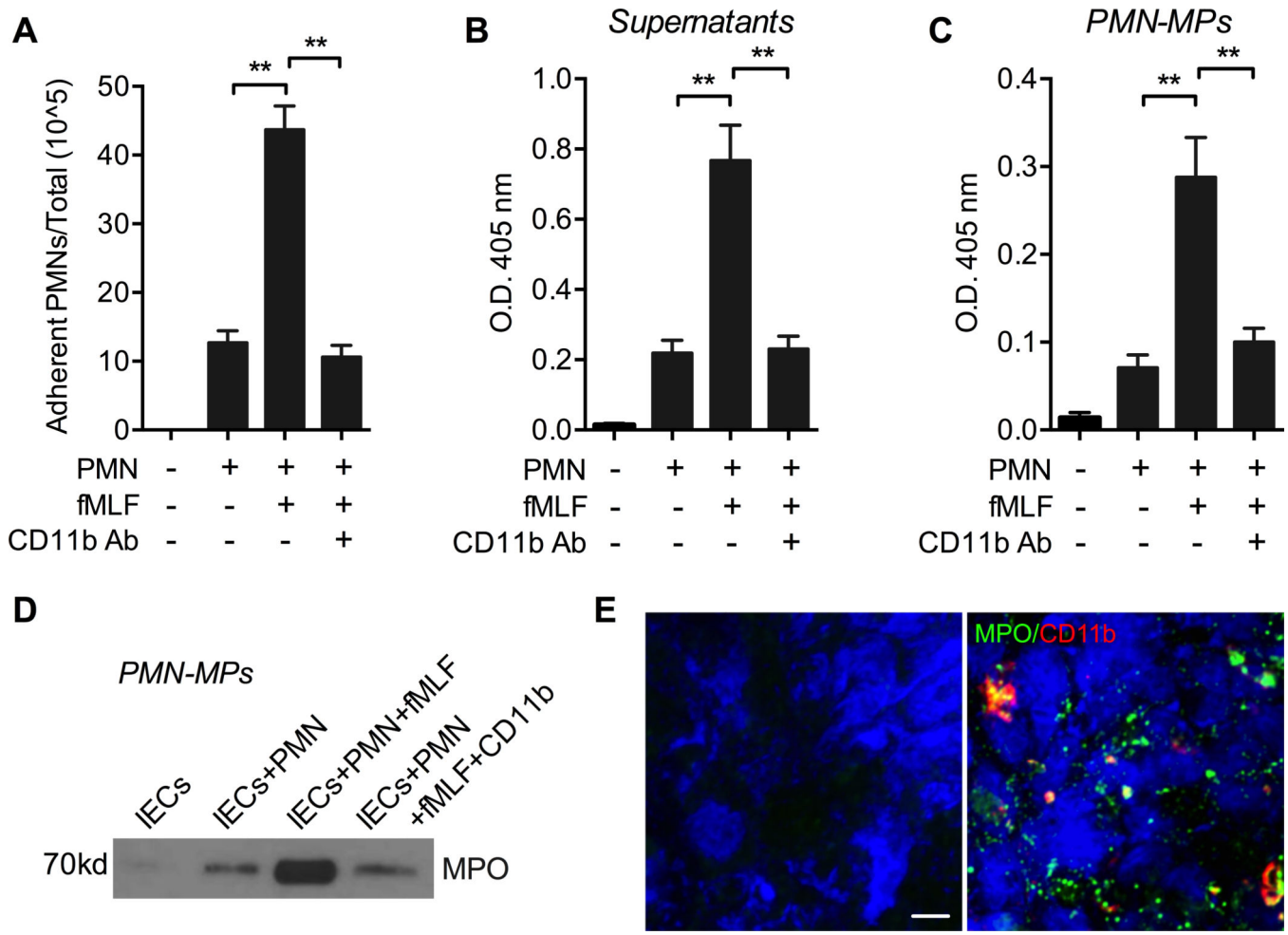

Figure 4. fMLF-induced adhesion of human PMNs to IECs triggers the release of MPO

Human PMNs (1×10^6) were introduced to IEC monolayers (grown in 12 well tissue culture plates, ratio of 1 adherent PMN to 2 IEC cells) and allowed to adhere for 3 hours at 37°C in the presence or absence of a low concentration of fMLF (100nM) and/or PMN adhesion inhibitory anti-CD11b Ab (10μg/ml). Supernatants from the co-cultures were collected and PMN-MPs were isolated form these supernatants. **(A)** fMLF treatment facilitates increased PMN adhesion to IECs, which was reversed with the inhibition of CD11b. ** $p<0.01$. **(B–D)** Peroxidase activity in supernatants of co-cultured PMNs and IECs **(B)** and on PMN-MPs **(C)** following fMLF-induced PMN adhesion to IECs was quantified using an ABTS peroxidase activity assay. ** $p<0.01$. For panels A-C data are presented as an average of 3 independent experiments. **(D)** MPO presence on PMN-MPs was further confirmed using immunoblotting analysis. Blots are representative of 3 independent experiments **(E)** PMN-MP binding to IECs following PMN adhesion was examined using fluorescence microscopy. Representative immunofluorescence images show a robust attachment of MPO positive aggregates (green) consistent with the size of PMN-MPs (> 1μm) to IECs (visualized using DAPI nuclear stain, blue). PMNs were stained for CD11b (red). Images are representative of 3 independent experiments. The bar is 10μm.

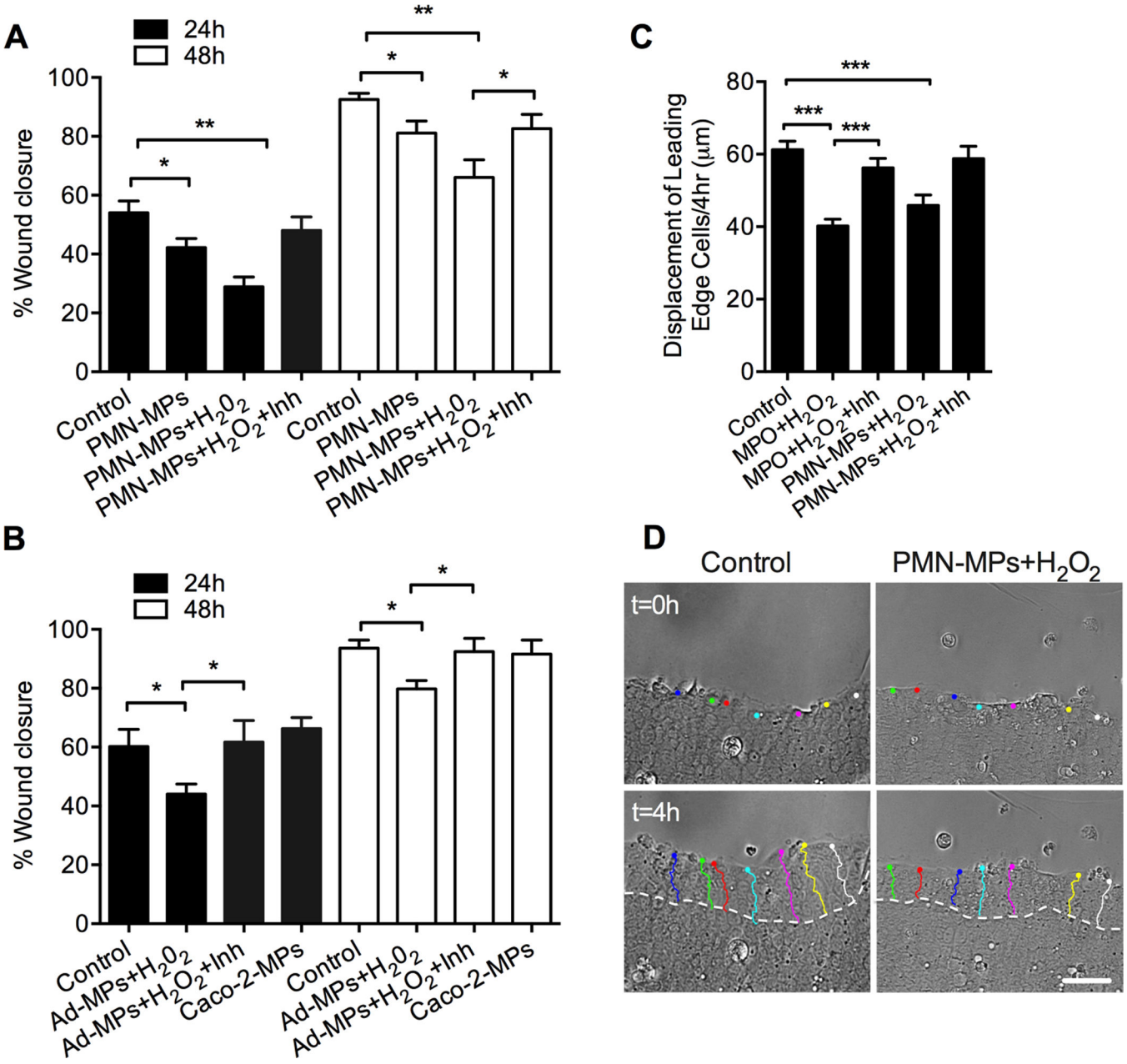

Figure 5. MP-associated MPO impairs wound healing of human IECs

(A) Scratch wound assays were performed to examine the effect of PMN-MPs on IEC wound closure. PMN-MPs (derived from 3×10^6 PMNs) were added to scratch wounded IEC monolayers with or without the addition of H_2O_2 and an MPO inhibitor. PMN-MPs and H_2O_2 treatment significantly decreased IEC wound closure both 24 and 48 hours post wounding. PMN-MPs effect was significantly decreased in the presence of MPO inhibitor (MPO Inhibitor I, 1μg/ml). * $p<0.05$, ** $p<0.01$. Data are presented as an average of 3 independent experiments. (B) Effect of PMN-MPs released following PMN adhesion to IECs (Ad-MPs) on IEC wound repair was investigated. PMNs (3×10^6) were introduced to IEC monolayers (grown in 6 well tissue culture plates) and allowed to adhere for 3 hours at

37°C in the presence of a low concentration of fMLF (100nM). Supernatants from co-cultures were collected and isolated MPs (derived from 3×106 PMNs) were added to scratch wounded IEC monolayers in the presence of H_2O_2. Ad-MPs and H_2O_2 treatment significantly decreased IEC wound closure both 24 and 48 hours post wounding. * $p<0.05$. Data are presented as an average of 3 independent experiments. **(C, D)** Time-lapse imaging analyses were performed to track the displacement of the leading edge IECs under the specified conditions. **(C)** Quantification of the displacement of leading edge cells at the wound (at least 50 cells/condition, from 3 independent experiments). The migratory capacity of leading edge cells was significantly decreased following treatments with either recombinant MPO or PMN-MPs in the presence of H_2O_2. *** $p<0.001$. **(D)** Representative bright field images (n=3) of migrating IEC monolayers with outlined tracks of leading edge cells without (left panels) or with (right panels) PMN-MPs/H_2O_2 treatment. The bar is 50μm.

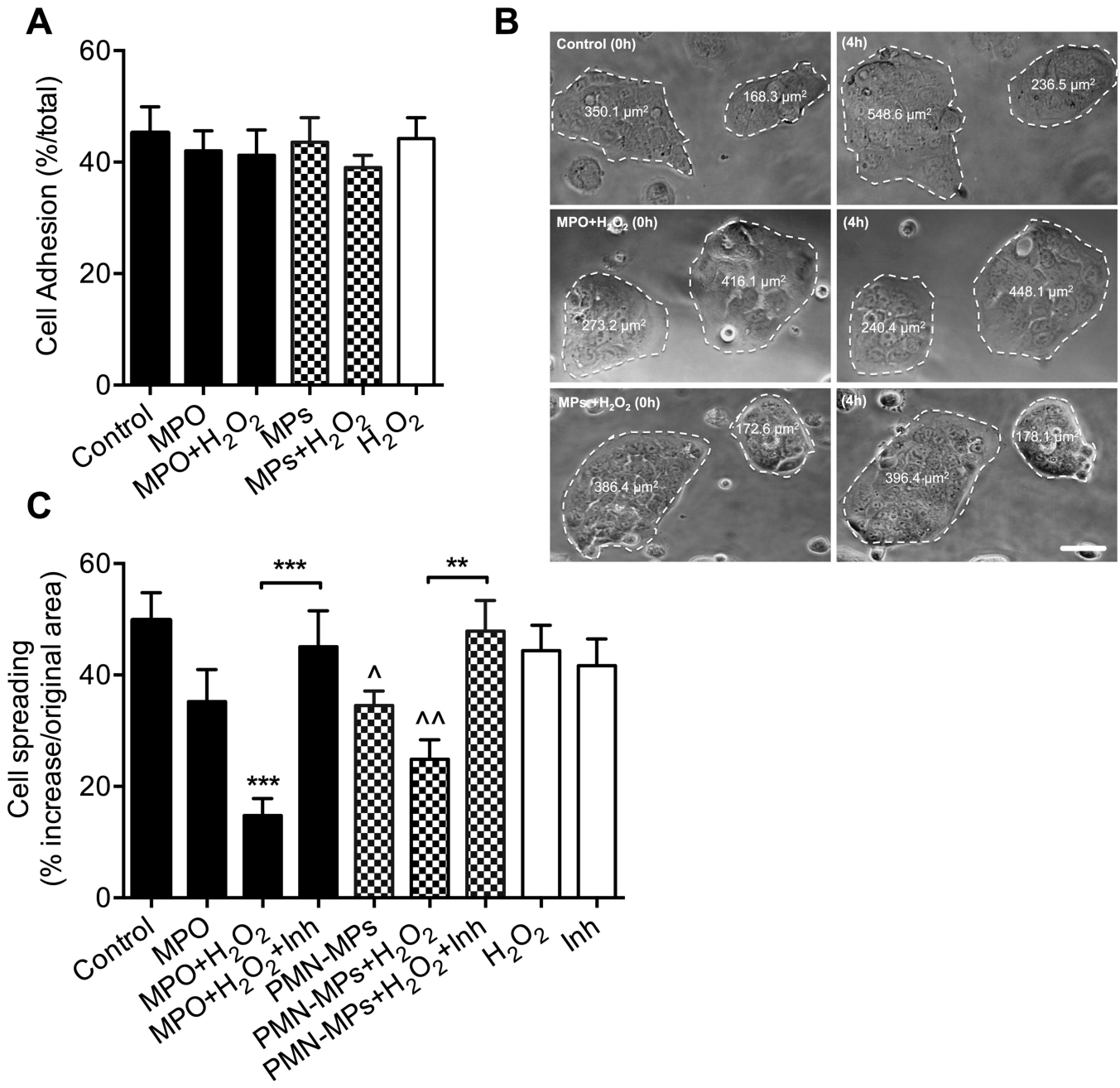

Figure 6. Recombinant and PMN-MP associated MPO suppress IEC migration by inhibiting IEC spreading

(A) Cell adhesion assay, where 150,000 cells/condition were allowed to adhere to Matrigel coated plates (1h, 37°C) was used to examine IEC-matrix adhesion after treatment with recombinant MPO or PMN-MPs with or without H_2O_2. No significant differences were observed. **(B–C)** Subconfluent IECs monolayers (~40% confluency) were allowed to spread on 13-mm collagen-coated coverslips for 4 hours following the specified treatments. The area of cellular clusters was measured before and after treatment. **(B)** Representative bright filed images (n=3 independent experiments) show inhibition of IECs spreading following MPO and PMN-MPs in the presence of H_2O_2. The bar is 50 µm. **(C)** Quantification of IEC

spreading under the specified conditions. Decreases in IEC spreading mediated by MPO and PMN-MPs in the presence of H_2O_2 were reversed with the addition of MPO inhibitor. Data are presented as percent increase in cell area measured at t=4h over t=0. ^ $p<0.05$, ^^ $p<0.05$ significantly different from control group, ** $p<0.01$.

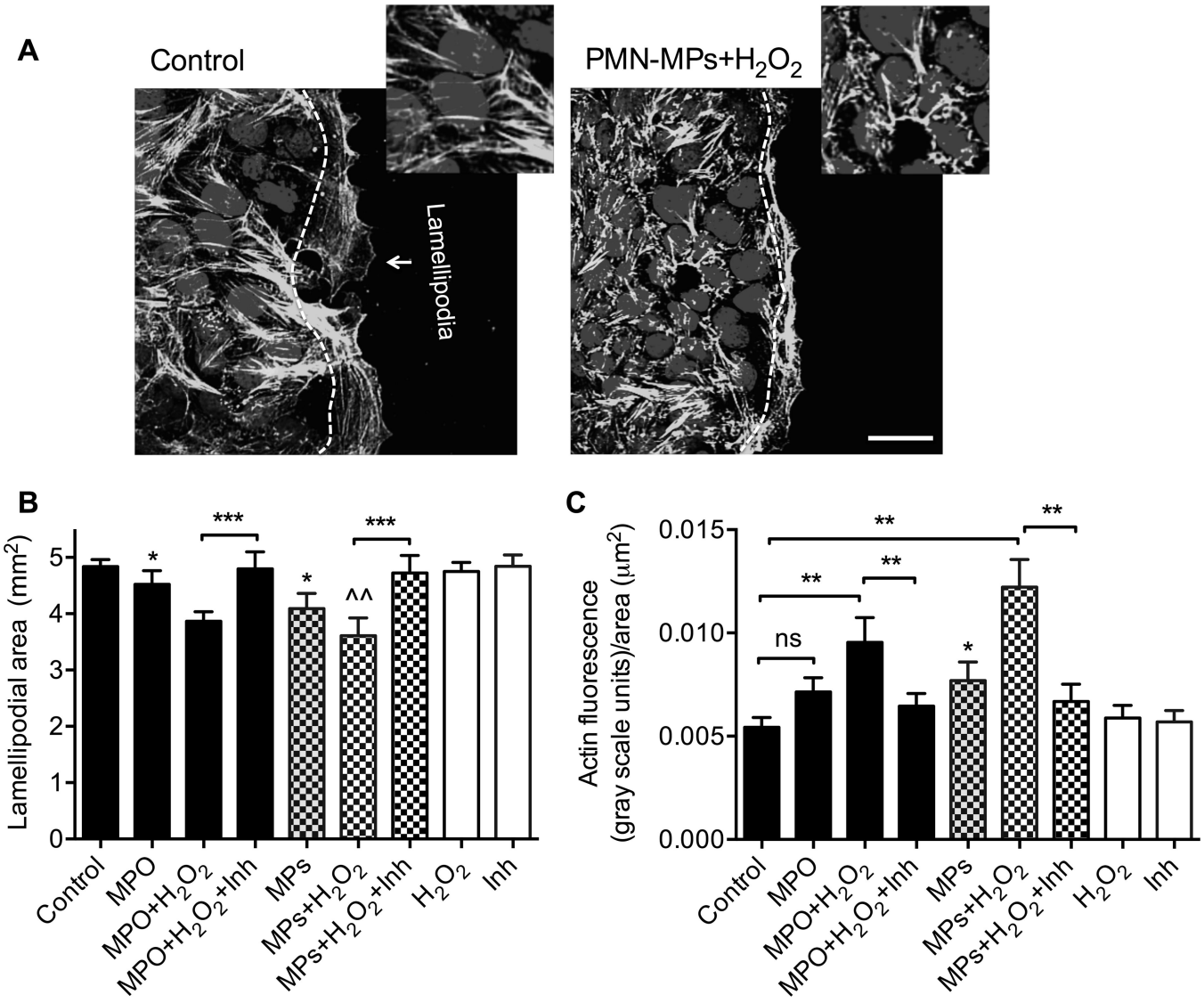

Figure 7. Recombinant and PMN-MP associated MPO inhibit lamellipodial extrusions and actin dynamics in migrating IECs

To examine the effect of soluble and PMN-MP associated MPO on lamellipodia formation and actin organization, scratch wounded cell monolayers were treated as indicated and allowed to migrate for 24 hours. At this time, IECs were fixed and stained for F-actin (green) and nuclei (blue). **(A)** Representative images (n=3 independent experiments) depict extended lamellipodium formation in control migrating IECs, which was inhibited in the presence of PMN-MPs and H_2O_2. The bar is 50 μm. Zoom-in images show impaired actin filament organization following PMN-MPs and H_2O_2 treatment. **(B)** The area of the lamellipodium was defined as the area past the nuclei of leading edge cells, as indicated by the white dashed line and quantified following the indicated treatment. At least 5 random fields per each condition were analyzed. N = 4 independent experiments. * $p<0.05$, ^^ $p<0.01$ significantly different from control group *** ($p<0.001$). **(C)** Actin accumulation at the leading edge of migrating IECs, as seen in the zoom-in images in **(A)** was quantified by measuring the fluorescence intensities of the lamellipodial area. Data are presented as total

fluorescence intensity in gray scale units normalized to area of the lamellipodium. Significant actin accumulation in migrating IECs was observed following treatment with MPO/PMN-MP and H_2O_2, indicating impaired actin dynamics. ^{ns} not significant. * $p<0.05$, significantly different from control group. *** ($p<0.001$). For **B** and **C**, data are shown as averages of 3 independent experiments.

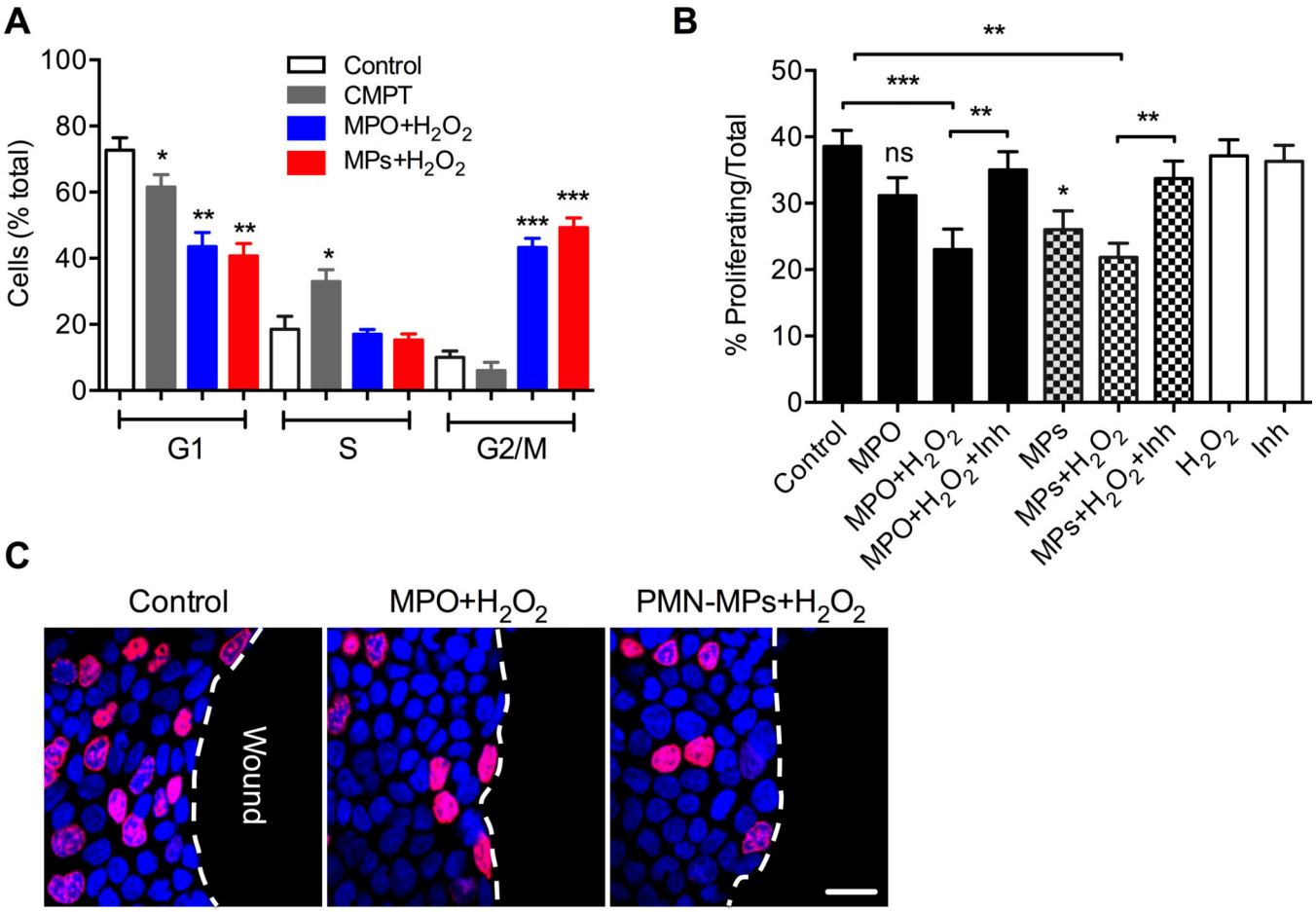

Figure 8. Recombinant and PMN-MP associated MPO inhibits IEC proliferation by inducing cell cycle arrest

The effect of soluble and MP-associated MPO on IEC proliferation was assayed using cell cycle analysis and Edu incorporation assay. **(A)** Propidium iodide staining and flow cytometry was used to perform cell cycle analyses of subconfluent IECs under the specified conditions. Treatment with either recombinant MPO or PMN-MPs with the associated MPO in the presence of H_2O_2 resulted in a significant accumulation of IECs in G2/M phase, suggesting cell cycle arrest. * $p<0.05$, ** ($p<0.01$), *** ($p<0.001$). Data are shown as averages of 3 independent experiments. **(B, C)** Proliferation of the leading edge cells in scratch wounded IEC monolayers was assessed by Edu incorporation. **(B)** At least 5 random fields per each condition were analyzed; the data are presented as % proliferating (nuclei stained in purple, EdU) with respect to total cells (nuclei stained in blue, topro-3) in the field. ^{ns} not significant. * different from control ($p<0.05$), ** ($p<0.01$), *** ($p<0.001$). **(C)** Images representative of three independent experiments show significantly decreased number of proliferating cells at the sites of closing wounds (wound edge) following treatment with either recombinant or PMN-MP associated MPO in presence of H_2O_2. Red (Edu, proliferative cells), Blue (Dapi, nuclei stain).

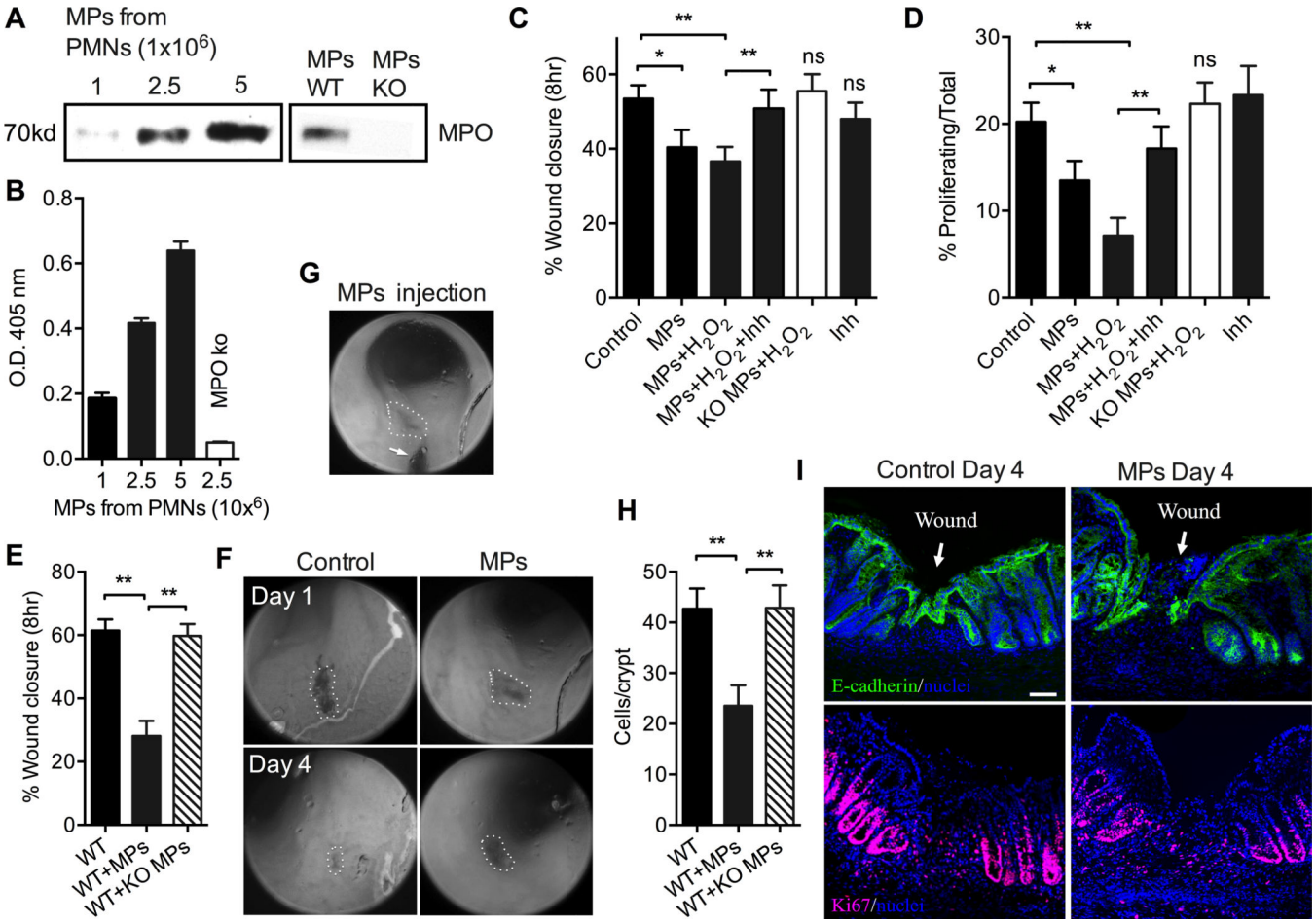

Figure 9. PMN-MPs mediate MPO-dependent inhibition of murine IEC proliferation and wound healing *in vitro* and *in vivo*

(A) MPO association with MPs isolated from increasing number of WT bone marrow-derived PMNs (as indicated, left panel) following sequential stimulation with Lt-B (1μM, 5min 37°C) and fMLF (5μM, 20min, 37°C) was confirmed by immunoblotting and compared to MPs isolated from MPO KO PMNs (MPs derived from 2×10^6 PMNs, right panel). **(B)** Activity of MPO associated with WT and KO PMN-MPs was examined by assaying for peroxidase activity, using ABTS as the substrate. MPs derived from increasing numbers of Lt-B/fMLF stimulated PMNs exhibited higher MPO activity, while as expected, MPs isolated from MPO KO PMNs had no enzymatic activity. **(C)** The effect of mouse PMN-MP-associated MPO on wound healing of murine IECs (CMT-93) was examined using scratch-wound assays. Treatment with WT PMN-MPs, but not with PMN-MPs derived from MPO KO PMNs, significantly inhibited IEC wound healing. The effect of WT PMN-MPs was reversed in the presence of an MPO inhibitor. * ($p<0.05$),** ($p<0.01$), ^{ns} not significant. **(D)** Proliferation of the leading edge cells in scratch wounded IEC monolayers was assessed by Edu incorporation. At least 5 random fields per each condition were analyzed; the data are presented as % proliferating/total cells. * ($p<0.05$), ** ($p<0.01$), ^{ns} not significant. **(E–I)** Superficial mucosal wounds were introduced to mouse colons using biopsy-based wound model. Twenty-four hours later murine PMN-MPs were microinjected

into the wounds. Mucosal wounds were visualized and measured using colonoscopic imaging at day 4 post-wounding. **(E)** Quantification of wound closure, ** $p<0.01$, and **(F)** representative images of mucosal wounds (outlined by dashed lines) days 1 and 4 post-wounding depict delay in mucosal wound healing following intraluminal administration of PMN-MPs into the wound area. **(G)** Representative image of PMN-MP microinjection site (arrow points to the injection needle). **(H–I)** Colonic mucosal wounds were extracted and OCT frozen. Eight-micrometer sections were stained for E-cadherin (green) or Ki67 (red) to visualize total and proliferating epithelial cells at wound edge. **(H)** Quantification of crypt cell proliferation (Ki67 positive cells, red, per crypt) and **(I)** Representative images show delayed re-epithelialization of wounded regions (upper panel) and decreased cell proliferation (bottom panel) following injection of PMN-MPs. 4′,6-diamidino-2-phenylindole (Dapi) was used to visualize cell nuclei. For panels **E-H** at least 12 wounds from 5 mice were used per condition.